Crossover behavior of the anomalous Hall effect in $Ga_{1-x}Mn_xAs_{1-y}P_y$ across the metal-insulator transition

Xinyu Liu [1,*] Sining Dong [1,2] Logan Riney [1] Jiashu Wang [1] Yong-Lei Wang,[1,2] Ren-Kui Zheng,[3] Seul-Ki Bac [1,4] Jacek Kossut [5] Margaret Dobrowolska,[1] Badih A. Assaf,[1] and Jacek K. Furdyna[1]

[1]*Department of Physics, University of Notre Dame, Notre Dame, Indiana 46556, USA*

[2]*Research Institute of Superconductor Electronics, School of Electronic Science and Engineering, Nanjing University, Nanjing 210093, China*

[3]*School of Materials Science and Engineering, Jiangxi Engineering Laboratory for Advanced Functional Thin Films, Nanchang University, Nanchang 330031, China*

[4]*Department of Physics, Korea University, Seoul, 136–701, Korea*

[5]*Institute of Physics, Polish Academy of Sciences, 02–668 Warszawa, Poland*

(Received 15 April 2021; accepted 2 June 2021; published 22 June 2021)

Quaternary alloy $Ga_{1-x}Mn_xAs_{1-y}P_y$ hosts magnetic and electronic properties that can be tuned by varying the P concentration "y", Mn concentration "x" and by annealing. In this work we make use of this tunability to probe the origin of the anomalous Hall effect (AHE) in $Ga_{1-x}Mn_xAs_{1-y}P_y$ thin films grown on GaAs that host perpendicular magnetic anisotropy. Specifically, we find that AHE in this class of materials is determined primarily by two contributions: an intrinsic band component arising from the Berry curvature, and a component determined by hopping conduction. As we vary the properties of $Ga_{1-x}Mn_xAs_{1-y}P_y$ from the metallic to the semi-insulating regime by changing the value of y and by postgrowth annealing, we observe a clear crossover from a Berry-curvature-induced AHE to one that is caused by hopping. The transition occurs approximately at the point where the numbers of localized and itinerant holes become comparable. In this hopping regime, the conductivity follows the Efros-Shklovskii scaling law versus temperature indicating the presence of a Coulomb gap, but the AHE remains robustly present. These results indicate that $Ga_{1-x}Mn_xAs_{1-y}P_y$ can host an interesting interplay between magnetism and Coulomb interactions.

DOI: 10.1103/PhysRevB.103.214437

I. INTRODUCTION

III-V-based ferromagnetic semiconductors, and particularly the ternary alloy $Ga_{1-x}Mn_xAs$, have been the object of intense investigation for nearly two decades, both for their novel physics and for the possibility of their device applications [1–3]. Ferromagnetism in these materials arises from the interplay between magnetic moments of Mn ions and of holes which arise from the presence of Mn [4,5]. While the information regarding the holes is frequently obtained from Hall effect measurements [6–8], Hall effect in ferromagnetic materials is modified by a strong contribution from the magnetization of the material, resulting in the so-called anomalous Hall effect (AHE). The physics of the AHE is, however, still not fully understood in this family of materials [9–12].

The arrival of the new quaternary alloy $Ga_{1-x}Mn_xAs_{1-y}P_y$, whose physical properties can be tuned by varying the concentration of phosphorus [13,14], offers several new advantages that can be exploited for understanding the origins of AHE in ferromagnetic semiconductors, and this is the goal of the present paper. Importantly, above 10 at. % of P, the strain in $Ga_{1-x}Mn_xAs_{1-y}P_y$ films grown epitaxially on GaAs substrates results in a magnetic easy axis in the film that is naturally oriented perpendicular to the film plane [15,16]. This enables one to readily obtain spontaneous magnetization normal to the film in AHE measurements, without the necessity of applying very high magnetic fields. Additionally, by varying the concentration of phosphorus, one has the tool for varying the energy gap of the material as well as the separation of the acceptor impurity band relative to the top of the valence band. This variation changes the ionization energy of acceptors, and can tune the density of charge carriers as well as the degree of their localization. These tuning knobs make $Ga_{1-x}Mn_xAs_{1-y}P_y$ ideal for studying the physics of AHE [17].

II. BACKGROUND AND OBJECTIVES

As is well known, in a ferromagnetic film the Hall resistivity ρ_{xy} is given by the sum of the ordinary Hall term ρ_{xy}^{O} and the anomalous Hall contribution ρ_{xy}^{A},

$$\rho_{xy} = \rho_{xy}^{O} + \rho_{xy}^{A} = R_0 B_z + R_s M_z, \tag{1}$$

where B_z is magnetic field applied normal to the sample plane, R_0 is the ordinary Hall coefficient $R_0 = 1/n_e e$ (where n_e is the carrier concentration), M_z is the component of magnetization $\boldsymbol{M}$ normal to the sample plane, and R_s is the anomalous Hall coefficient [18].

Several established processes can lead to the AHE. These processes are empirically identified by the way in which ρ_{xy}^{A}

*xliu2@nd.edu

TABLE I. Properties of $Ga_{0.94}Mn_{0.06}As_{1-y}P_y$ films (Refs. [16,17]).

P concentration y		0.10	0.15	0.21
Thickness d (nm)		48.3	74.3	47.2
Curie Temperature T_C (K)	Annealed	96	80	87
	As-grown	59	48	40
Total hole concentration ($\times 10^{20}$ cm^{-3})	Annealed	7.12	6.05	7.99
	As-grown	3.78	3.42	1.95
Free hole concentration ($\times 10^{20}$ cm^{-3})	Annealed	6.59	1.84	3.57
	As-grown	1.41	0.56	0.38

depends on the longitudinal resistivity ρ_{xx}. One mechanism, proposed by Karplus and Luttinger [19], arises purely from band-structure considerations, and predicts that ρ_{xy}^A varies as ${\rho_{xx}}^2$. This process, linked directly to topological properties of Bloch states, can be understood in terms of the Berry curvature [20,21], and is traditionally referred to as "intrinsic". Contributions to AHE can also arise from disorder- and impurity-scattering in ferromagnets, and are then referred to as "extrinsic". Two examples of such processes are skew scattering (which leads to a linear relation between ρ_{xy}^A and ρ_{xx}) and side-jump scattering (which leads to a dependence of $\rho_{xy}^A \propto {\rho_{xx}}^2$) [22]. Although the side jump process is proportional to ${\rho_{xx}}^2$, similar to the intrinsic mechanism identified above, it is much weaker [23,24], and we will neglect it in this paper. Importantly for the present context, Nagaosa *et al.* [18] noted that in the "bad-metal" or "hopping" regime ($\rho_{xx} > 0.1$ mΩcm), which corresponds to properties of many dilute ferromagnetic alloys (including many ferromagnetic semiconductors [6,11,12]), the dependence of ρ_{xy}^A on ρ_{xx} can be described experimentally by the universal relation $\rho_{xy}^A \propto {\rho_{xx}}^{0.4}$. Although a wide range of ferromagnetic materials obey this scaling relation, its theoretical mechanism in magnetic III-V materials is not fully understood, representing a major challenge for AHE theory [25].

In this work we utilize the P concentration in $Ga_{1-x}Mn_xAs_{1-y}P_y$ as a knob to tune the AHE from the low-resistivity metallic regime, where it is dominated by the intrinsic contribution, to the high-resistivity regime, where it is dominated by hopping. The systematic tuning of the P concentration y and of the carrier density at fixed value of x allows us to study the weight of these two coexisting contributions to AHE in the presence of a concentration of holes that can be additionally controlled by annealing. We find that the metallic contribution is dominant when charge carriers populate an impurity band that is in close proximity of the valence band. As the phosphorus concentration y increases, and the valence band is pushed down in energy further away from the impurity band, the hopping contribution to AHE gradually becomes dominant. This regime approaches a metal-insulator transition at low temperature and Coulomb interactions become significant.

III. EXPERIMENTAL PROCEDURE

$Ga_{1-x}Mn_xAs_{1-y}P_y$ films with a fixed value of Mn concentration of $x = 0.06$ and with phosphorus concentrations $y = 0.10$, 0.15, and 0.21 were grown on semi-insulating GaAs (100) substrates using low-temperature molecular beam epitaxy. Parts of the films were then annealed at 270 °C for 1 h in nitrogen flux to optimize their uniformity and to improve their magnetic properties. Manganese and phosphorus concentrations, film thicknesses, Curie temperatures, and saturation magnetizations of the specimens used in this study were characterized and have been published in an earlier paper [16]. For electrical transport measurements, Hall bars were fabricated by photolithography, with the long dimension (the current direction) along the [110] orientation of the GaAs substrate. Measurements of Hall resistivity ρ_{xy} and longitudinal resistivity ρ_{xx} were then performed as a function of magnetic field B (from zero to 12.0 T) and temperature (between 1.5 and 70 K) on all six specimens in a Physical Property Measurement System (PPMS). Table I summarizes the phosphorus concentrations, thicknesses, saturation magnetizations, Curie temperatures, free hole concentrations, and conductivities of all $Ga_{1-x}Mn_xAs_{1-y}P_y$ films used in this study [17].

IV. EXPERIMENTAL RESULTS AND ANALYSIS

Figure 1 shows ρ_{xy} and ρ_{xx} results measured on the annealed $Ga_{0.94}Mn_{0.06}As_{0.85}P_{0.15}$ sample. Results on the other five specimens are very similar. Note that at temperatures well below Curie temperature the value of ρ_{xy} is nearly constant as a function of field, indicating that ρ_{xy} is strongly dominated by the spontaneous perpendicular magnetization of the samples, as is typical for AHE in ferromagnets with magnetization perpendicular to the sample plane.

We recall from the preceding section that the anomalous Hall resistivity ρ_{xy}^A in a ferromagnetic material may contain

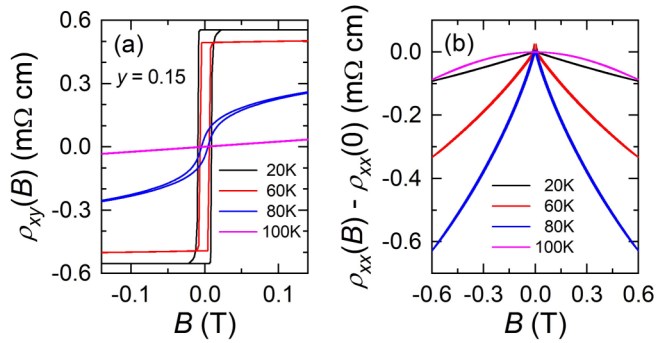

FIG. 1. Typical magnetic field dependence of (a) Hall resistivity ρ_{xy} and (b) longitudinal resistivity ρ_{xx} on perpendicular applied field at several temperatures for annealed GaMnAsP specimens with $y = 0.15$. $\rho_{xx}(0)$ is the zero-field resistivity at each temperature.

contributions from different mechanisms that can be identified empirically by their dependence on different powers of ρ_{xx}. Our purpose in this paper will be to identify the relative contributions from these mechanisms in $Ga_{1-x}Mn_xAs_{1-y}P_y$ samples under investigation. To accomplish this, we rewrite Eq. (1) in the form

$$\rho_{xy} - R_0 B = \rho_{xy}^A, \tag{2}$$

where ρ_{xy}^A indicates the contribution of magnetization to the Hall resistivity. The contributions of skew scattering, intrinsic and hopping mechanisms to ρ_{xy}^A can then be expressed as [18]

$$\rho_{xy}^A = aM\rho_{xx}, \tag{3}$$

$$\rho_{xy}^A = bM{\rho_{xx}}^2, \tag{4}$$

and

$$\rho_{xy}^A = cM{\rho_{xx}}^{0.4}, \tag{5}$$

where Eqs. (3)–(5) indicate relative strengths of the intrinsic ($b \neq 0$), skew scattering ($a \neq 0$) or hopping conduction ($c \neq 0$) contributions.

We can now rewrite ρ_{xy} in a form that contains a superposition of all three contributions discussed above,

$$\rho_{xy} = R_0 B + aM\rho_{xx} + bM{\rho_{xx}}^2 + cM{\rho_{xx}}^{0.4}. \tag{6}$$

However, as discussed in Nagaosa *et al.* [18], the contribution corresponding to skew scattering (i.e., $\rho_{xy}^A \propto \rho_{xx}$) requires highly ordered crystals, with high conductivity and very long relaxation times, which is not satisfied in the ferromagnetic semiconductors of the $Ga_{1-x}Mn_xAs$ family. We will, therefore, eliminate the second term on the right-hand side of Eq. (6). We then have

$$\rho_{xy} = R_0 B + bM{\rho_{xx}}^2 + cM{\rho_{xx}}^{0.4}, \tag{7}$$

which we can now use to determine the degree to which each of the two remaining mechanisms contributes to AHE, by fitting Eq. (7) to our experimental results and obtaining the intrinsic and hopping coefficients, b and c.

For this purpose, we rewrite Eq. (7) in the form [26,27]

$$(\rho_{xy} - R_0 B)/({\rho_{xx}}^{0.4}M) = \rho_{xy}^A/({\rho_{xx}}^{0.4}M) = c + b{\rho_{xx}}^{1.6}, \tag{8}$$

where ρ_{xy}^A is the AHE contribution to ρ_{xy} as defined in Eq. (1). By plotting $(\rho_{xy} - R_0 B)/({\rho_{xx}}^{0.4}M)$ as a function of ${\rho_{xx}}^{1.6}$, we then obtain the coefficient c from the intercept of the plot, and coefficient b from its slope. We note that the value of R_0, which represents the concentration of itinerant holes in the material, has already been obtained for each of the six samples in an earlier study [17]. Since we are dealing with a heavily doped semiconductor, it is safe to assume that this quantity will remain constant as temperature and field are varied.

Note that the quantities ρ_{xy} and ρ_{xx} which will be used in plotting $(\rho_{xy} - R_0 B)/({\rho_{xx}}^{0.4}M)$ as a function of ${\rho_{xx}}^{1.6}$ were measured at a series of temperatures T (from 1.5 to 70 K) and magnetic fields B (from 0 to 12.0 T), and the value of M to be used in these plots must therefore correspond to each value of B and T at which ρ_{xy} and ρ_{xx} were measured. To achieve that, we develop a modified Weiss-Brillouin model for the magnetization $M(B,T)$ in the Appendix. As discussed in the Appendix, the model follows the Weiss-Brillouin approach as modified by Harrison [28].

A. Analysis of AHE in annealed samples of $Ga_{1-x}Mn_xAs_{1-y}P_y$

We begin our analysis of intrinsic and hopping contributions to AHE in $Ga_{1-x}Mn_xAs_{1-y}P_y$ by investigating the results obtained in annealed samples, which are made much more uniform by this process. Using Eq. (7) and the values of $m(B,T) = M(B,T)/M_0$ (M_0 is the value of total magnetization) as discussed in the Appendix, we plot $(\rho_{xy} - R_0 B)/({\rho_{xx}}^{0.4}M)$ vs ${\rho_{xx}}^{1.6}$ [panels (a)–(c) in Fig. 2] to determine the coefficients b and c.

Having determined the values of the coefficients b and c in Eq. (7), we can now establish the relative contributions of, respectively, the intrinsic and hopping mechanisms to AHE in annealed $Ga_{1-x}Mn_xAs_{1-y}P_y$ samples. To eliminate the effect of changes in M, we do this by plotting $(b{\rho_{xx}}^2)/m$ and $(c{\rho_{xx}}^{0.4})/m$ as a function of ρ_{xx} in Figs. 2(d)–2(f), where $m = M/M_0$ and M_0 is the value of total magnetization, which is a constant for each sample. It is clear from Fig. 2 that in all annealed specimens the intrinsic mechanism dominates the AHE process. It is interesting that earlier studies of AHE in annealed GaMnAs with similar Mn concentrations have also led to ρ_{xy}^A values that follow an approximately ${\rho_{xx}}^2$ dependence, also indicating dominance of intrinsic processes in AHE [8,24,29–31].

B. Analysis of AHE in as-grown samples of $Ga_{1-x}Mn_xAs_{1-y}P_y$

We will now analyze the results obtained for the as-grown $Ga_{1-x}Mn_xAs_{1-y}P_y$ samples, again by starting with Eq. (7) and following the same procedure used in the preceding section. The results are displayed in Fig. 3, where we obtain coefficient b and c for each as-grown sample from the slope and intercept in panels (a)–(c), and plot the resulting intrinsic and hopping contributions to AHE separately in panels (d)–(f). It is immediately apparent that the results for the as-grown samples are significantly more complex than those in Fig. 2.

The behavior of the as-grown $Ga_{0.94}Mn_{0.06}As_{0.90}P_{0.10}$ sample is still qualitatively similar to that of annealed specimens, displaying clear dominance of the intrinsic component of AHE, as seen in Fig. 3(d). However, the difference between as-grown and annealed samples becomes increasingly complicated as the phosphorus content increases. In the case of our largest phosphorus concentration, sample $Ga_{0.94}Mn_{0.06}As_{0.79}P_{0.21}$, the role of intrinsic and hopping contributions in the as-grown case has now become reversed, as seen in Fig. 3(f), the hopping contribution $cM{\rho_{xx}}^{0.4}$ becoming dominant. This sample then displays a behavior corresponding to the regime identified by Nagaosa *et al.* as the "hopping regime" [18]. Interestingly, the results for the $Ga_{0.94}Mn_{0.06}As_{0.85}P_{0.15}$ sample shown in Fig. 3 fall between the two as-grown specimens just described, showing that magnitudes of hopping and intrinsic contributions to AHE are comparable, thus corresponding to crossover conditions between the two AHE mechanisms.

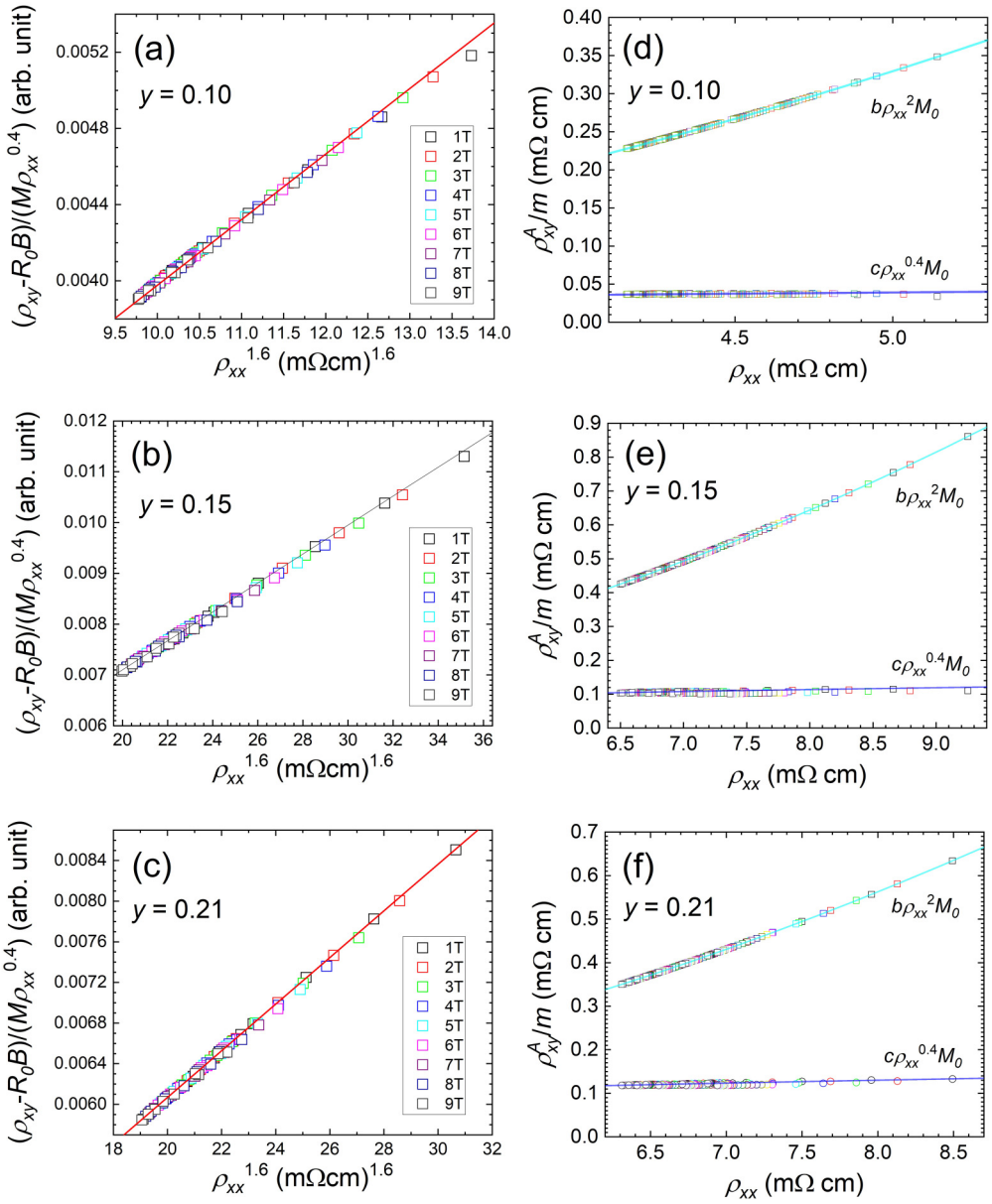

FIG. 2. (a),(b),(c) Plot of $(\rho_{xy}\text{-}R_0B)/(M\rho_{xx}^{0.4})$ vs $\rho_{xx}^{1.6}$ for the annealed $Ga_{1-x}Mn_xAs_{1-y}P_y$ samples with P concentrations y of 0.10, 0.15, and 0.21. The slope is b, the y-axis intercept is c. (d),(e),(f) The two components of ρ_{xy}^A, $b\rho_{xx}^2M_0$ and $c\rho_{xx}^{0.4}M_0$, are plotted separately as a function of ρ_{xx} for each annealed $Ga_{1-x}Mn_xAs_{1-y}P_y$ sample using the values of b and c obtained from (a),(b),(c). Here M_0 is the saturation magnetization at $T = 0$ K, and m is the normalized magnetization $M(B, T)/M_0$ as given by the modified Weiss-Brillouin function in the Appendix.

C. Crossover into the hopping regime and its nature

In Fig. 4, we are now able to plot the variation of σ_{xy} as a function of σ_{xx} for all six samples studied here. As seen in that figure, the conductivity covered in this study spans two orders of magnitude, and the scaling of σ_{xy} vs σ_{xx} follows two different but clearly identifiable regimes. (i) At low conductivities, $\sigma_{xy} \sim \sigma_{xx}^{1.6}$, corresponding to the hopping regime dominated by impurity band transport [25]. (ii) At high conductivities the value of σ_{xy} is approximately constant, corresponding to the intrinsic (metallic) regime dominated by the Berry curvature contribution to AHE [23] .We note parenthetically that, as shown in Supplemental Material [32], a similar universal scaling crossover as a function of sample conductivity is also followed in the parent ferromagnetic alloy $Ga_{1-x}Mn_xAs$ [11].

We can tie the occurrence of the observed crossover to the changing carrier density of the system and the increased isolation of the impurity band as the P concentration increases. According to our previous work [17] a large fraction of holes ($\sim 6\times10^{19}$ cm^{-3}) are localized in $Ga_{1-x}Mn_xAs_{1-y}P_y$, and do not contribute to conduction. Note that in samples that are in the hopping regime, the delocalized hole density measured by the normal Hall effect (see Table I) is lower than this threshold. While there remains a finite concentration of free carriers, they no longer constitute the majority. Thus, it is

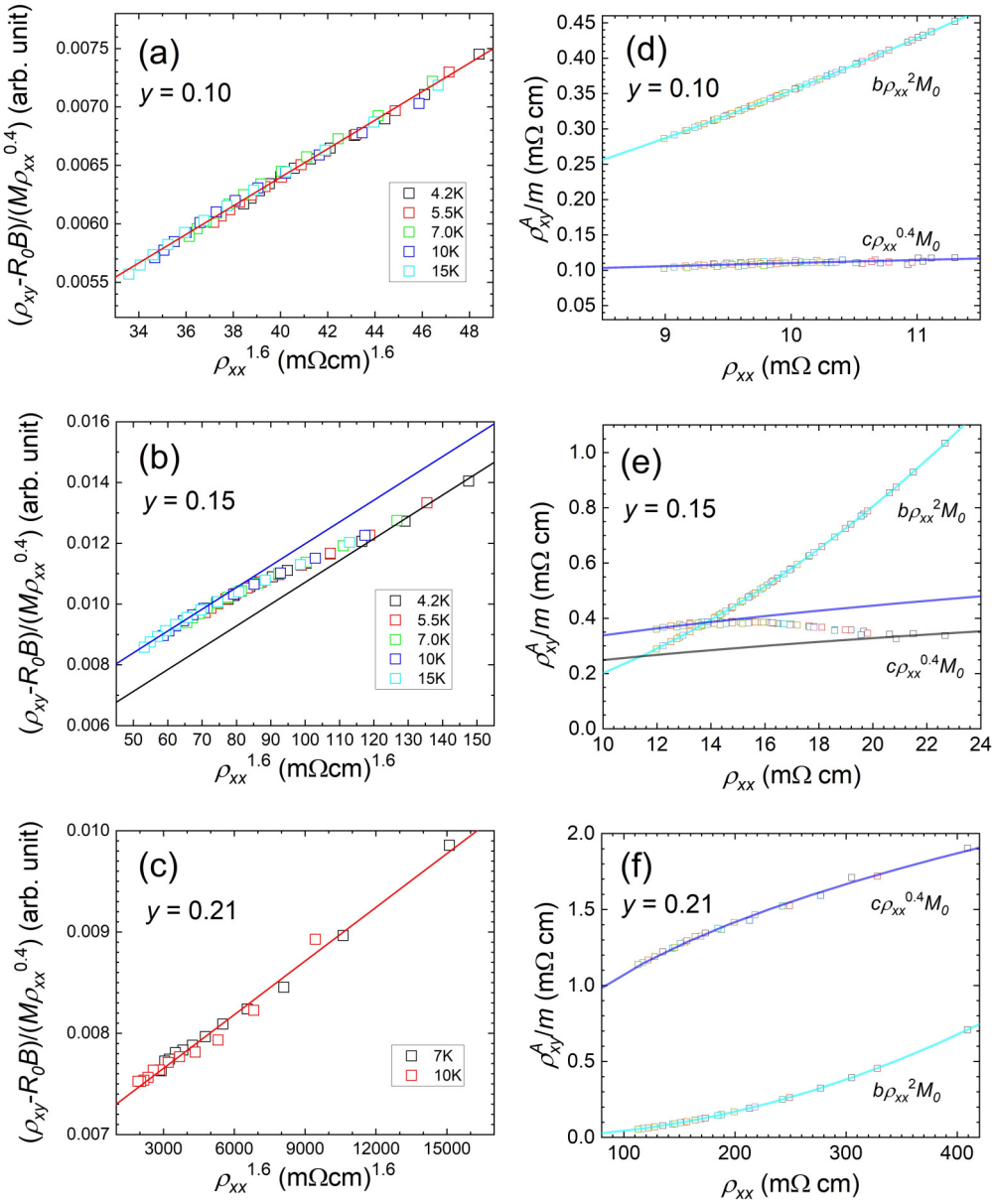

FIG. 3. (a),(b),(c) Plot of $(\rho_{xy}\text{-}R_0B)/(M\rho_{xx}{}^{0.4})$ vs $\rho_{xx}{}^{1.6}$ for as-grown $Ga_{0.94}Mn_{0.06}As_{1-y}P_y$ samples with $y = 0.10$, 0.15, and 0.21, respectively. The slope is b, the y-axis intercept is c. (d),(e),(f) Intrinsic and hopping components of AHE, $b\rho_{xx}{}^2M_0$ and $c\rho_{xx}{}^{0.4}M_0$, plotted separately for the three as-grown samples.

likely that the crossover occurs when the concentrations of free and localized holes become comparable.

Since the two samples with the lowest hole density approach the localization threshold, we further examine the temperature dependence of their resistivity versus temperature in Figs. 5(a) and 5(b). This allows us to get further insight into the nature of the metal-insulator transition that these specimens undergo at low temperature, and into the eventual role of Coulomb interactions [33]. In the presence of carrier screening, it was shown that the dependence of resistivity on temperature in the localized regime follows the following scaling relation [34,35]:

$$\rho_{xx}(T) \sim T^{\nu} \exp\left(\frac{T_0}{T}\right)^{s}, \tag{9}$$

where ν is a nonuniversal exponent that accounts for the power-law dependence of the resistivity on the temperature [35], and T_0 is the characteristic temperature related to the localization length ξ or activation energy. The value of s is indicative of the type of localization regime: $s = 1/4$ corresponds to Mott variable-range hopping [36], with the localization length defined by $\xi = (\gamma/g_0k_BT_0)^{1/2}$, where γ is a constant, g_0 is the density of the states, and k_B is the Boltzmann constant, and $s = 1/2$ applies in the presence of a Coulomb gap [37], with the localization length in this case defined by $\xi = Ce^2/\kappa k_BT_0$, where C is a constant, and κ is the dielectric constant; and $s = 1$ applies in the presence of mechanisms such as a mobility gap [38].

Figure 5(a) shows the agreement of $\rho_{xx}(T)/T^{\nu}$ with the $s = 1/4$ rule for the as grown $y = 0.15$ sample at different

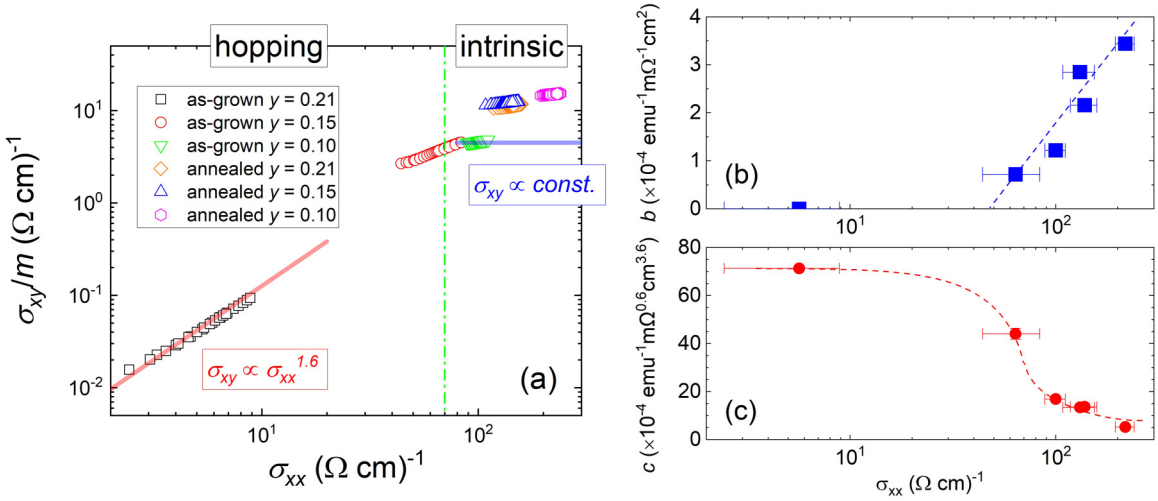

FIG. 4. (a) Phase diagram of the anomalous Hall effect versus sample conductivity. Two regimes can be distinguished: the hopping regime, where $\sigma_{xy} = c{\sigma_{xx}}^{1.6}M_0$ is dominant; and the intrinsic regime, where σ_{xy} is dominated by bM_0. Note that the number of points in the high-conductivity data is the same as at low conductivities, but are squeezed together by the logarithmic scale. (b),(c) Variation of the coefficients b (Berry curvature contribution) and c (hopping contribution) as a function of sample conductivity. The dashed lines are guide for eyes.

magnetic fields. This sample is at the boundary between the hopping and metallic regime. However, $\rho_{xx}(T)$ indicates strong evidence of a Mott-like activation upon the onset of localization [39]. Figure 5(b), on the other hand, shows agreement of $\rho_{xx}(T)/T^{v}$ with the $s = 1/2$ rule for the as-grown $y = 0.21$ sample at different magnetic fields. This sample exhibits the strongest metal-insulator transition, but also exhibits evidence of a Coulomb gap [40,41]. Note that T_0 decreases at high magnetic field. This indicates that a magnetic field induces a delocalization effect, similar to what is discussed in an earlier work in a gated GaAs/$Al_xGa_{1-x}As$ heterostructure [34]. In a magnetic semiconductor this effect can also be associated with the reduced spin-disorder scattering of carriers as the magnetic field increases [42].

V. DISCUSSION

As shown by earlier theoretical calculations [25], the nature of the hopping regime cannot be inferred from the anomalous Hall effect alone. However, the combined investigation of scaling of both ρ_{xx} and ρ_{xy} sheds important light on the nature of the interactions that compete or cooperate to generate the AHE in $Ga_{1-x}Mn_xAs_{1-y}P_y$. Our results indicate that both a metallic and hopping contributions contribute to the AHE in this material, and that the weight of each contribution can be tuned by varying the phosphorus concentration y, the conductivity, or both. In the metallic regime the AHE is dominated by the intrinsic contribution arising from the Berry curvature. Once the impurity band is sufficiently far from the valence band (as for $y = 0.21$), the AHE is mainly governed by the hopping contribution. At the boundary between the two regimes, the conductivity follows the Mott variable range hopping law, but as samples become more insulating, Coulomb interactions become significant and the conductivity follows the Efros-Shklovskii rule.

Whether or not Coulomb interactions contribute significantly to hopping conduction generally depends on the size of the Coulomb gap compared to the hopping energy. The single particle density-of-state can influence of both energy scales. The presence of screening from a nearby metallic band can also decrease the weight of the Coulomb interaction. Thus, it is difficult to isolate one reason why these interactions only start to be significant as the P content is increased, since both the band structure and the conductivity are altered by the introduction of P. Unexpectedly an important question emerges from our work: is there a regime in ferromagnetic semiconductors in which the Berry curvature and Coulomb interactions cooperate to generate correlated topological effects [43,44]?

We note here that an intense discussion regarding the role of the impurity band (IB) in $Ga_{1-x}Mn_xAs$, including the position of the Fermi energy, has arisen in analyzing its ferromagnetic properties [45]. The incorporation of Mn in a III-V lattice results in holes that reside in an IB above the top of the valence band (VB). At Mn concentrations typical of this family of ferromagnetic semiconductors (up to 10 at. % and more) the number of states in the impurity band, and thus its width, is given by the quantity $(x_{sub}–x_{int})$, where x_{sub} and x_{int} are concentrations of substitutional and interstitial Mn [46]. This is a very large number, resulting in significant broadening of IB [47,48]. In the specific case of $Ga_{1-x}Mn_xAs$, in which IB lies about 100 meV above the top of the VB [49], such broadening can lead to an overlap of IB with the top of VB, resulting in effect in one continuous band, with the Fermi level determined by the concentration of interstitials [46] lying inside this combined IB/VB. In the case of $Ga_{1-x}Mn_xAs_{1-y}P_y$, however, the top of the valence band itself will shift downward relatively fast in energy as y increases, thus reducing the overlap of IB with VB, and eventually very likely leading to their separation. This may in fact be the mechanism which underlies the transition from the Berry phase to the hopping regime reported in this paper. While we cannot make a definitive statement at this time, further study of $Ga_{1-x}Mn_xAs_{1-y}P_y$ with high values of y would clearly be beneficial to increase our understanding both of the hopping process and of the role of IB.

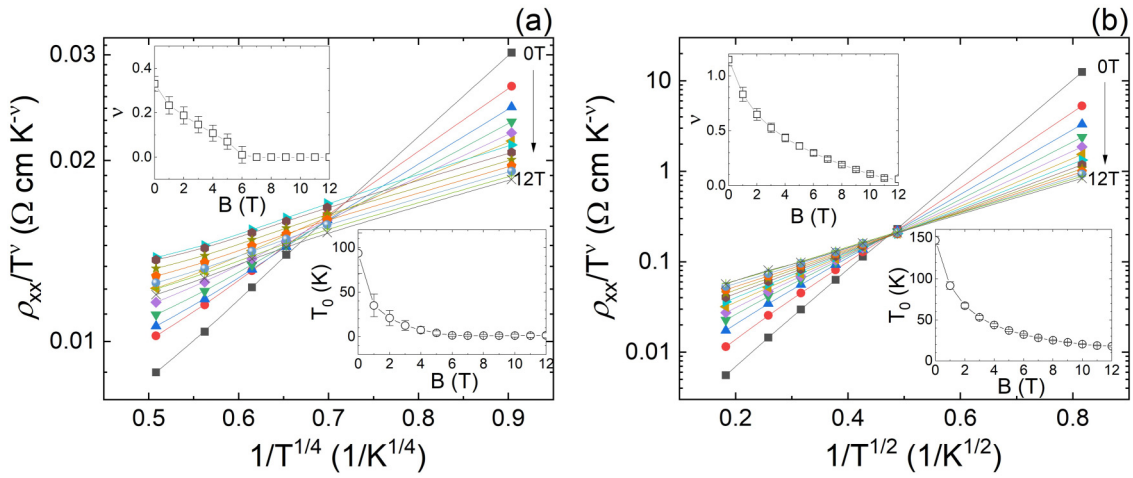

FIG. 5. (a) Scaling of the resistivity vs $T^{-1/4}$ in the as-grown $y = 0.15$ sample at different magnetic fields. (b) Scaling of the resistivity vs $T^{-1/2}$ in the as-grown $y = 0.21$ sample at different magnetic fields. Insets show the temperature dependence of ν and T_0.

We have shown here that $Ga_{1-x}Mn_xAs_{1-y}P_y$ allows us to tune three quantities: the magnetic moment (Mn/Ga), the carrier density (P and annealing), and the position of the impurity band with respect to the valence band (As/P). Thus, a proper mapping of the phase diagram of this material can be a route for investigating the interplay between topological Berry curvature effects, disorder, and strong correlations [43,44].

ACKNOWLEDGMENTS

This work was supported by the National Science Foundation Grant No. DMR 1905277, the National Natural Science Foundation of China (Grants No. 61971464 and No.11974155), and the National Key R&D Program of China (Grant No. 2018YFA0209002).

APPENDIX: DERIVATION OF $M(B, T)$ BY MODIFIED WEISS-BRILLOUIN MODEL

As noted in the main text, resistivities ρ_{xy} and ρ_{xx} were measured at a series of temperatures T and magnetic fields B, and our analysis of these quantities requires the use of magnetization $M(B, T)$ corresponding to the values of B and T at which ρ_{xy} and ρ_{xx} were measured. To obtain $M(B, T)$, in this Appendix we will use the mean-free field model of Weiss-Brillouin as modified by Harrison [28,50], in the form

$$m = \frac{M}{M_0} = B_J[\beta g J \mu_0 \mu_B (H + \alpha M)/kT], \qquad \text{(A1)}$$

where $B_J(x)$ is the Brillouin function,

$$B_J(x) = c_J \coth(c_J x) - d_J \coth(d_J x). \qquad \text{(A2)}$$

Here $c_J = (2J + 1)/(2J)$, $d_J = 1/(2J)$, M is magnetization at any given field B and temperature T, and M_0 is the value of the magnetization when all magnetic moments are parallel to the external field, i.e., the maximum value that magnetization can attain. M_0 can be written as $M_0 = Ng\mu_B J$, where N is the number of spins per unit volume in the material, g is the g factor, μ_B is the Bohr magneton, μ_0 is the permeability of vacuum, and in our case $g = 2$ and $J = 5/2$. Note further that in Eq. (A1) parameter α is the standard exchange field coefficient, and β is the domain coefficient introduced by Harrison [50].

As a start, we solve the implicit Eq. (A1) for $M(B, T)$, as follows. We assume that the quantity M_0 is given by the value of M measured at our lowest temperature (in our case 3 K) at a field of 7.0 T, as listed for each sample in Table I. We then set the applied field H to zero in Eq. (A1), input the measured value of M_0 and remanent magnetization $M(0, T)$ at a given temperature as shown in the Supplemental Material [32] (blue curve in Fig. S3), and solve Eq. (A1) for the product $\alpha\beta$. For comparison, in Fig. S3 we also plot $M(0, T)$ calculated using the classical mean field model, in which the value of $\alpha\beta = 3kT_C/[g\mu_0\mu_B(J + 1)M_0]$, illustrating the importance of determining the coefficients α and β for each temperature. We do this by adjusting the value of $\alpha\beta$ at each temperature, so that calculated remanent magnetization $M_r = M(0, T)$ obtained by setting $H = 0$ in Eq. (A1) at that temperature equals the measured value of $M(0, T)$ for each sample. This process yields the value of the product $\alpha\beta$ for each sample at each temperature.

To complete the modified mean field model for $M(B, T)$ in Eq. (A1), we now need to separately establish the value of the domain coefficient β. To illustrate the process, in Fig. S4 (in the Supplemental Material [32]) we first plot $(\rho_{xy} - R_0 B)/(M\rho_{xx}{}^{0.4})$ vs $\rho_{xx}{}^{1.6}$ for the $y = 0.15$ sample for $\beta = 1$. We note that the slopes of the curves for different temperatures are the same, attesting to the robustness of the intrinsic coefficient b, but the series of curves have different intercepts. Since we assume that the coefficient c, which governs the hopping contribution to AHE and which corresponds to the intercept of $(\rho_{xy} - R_0 B)/(M\rho_{xx}{}^{0.4})$ vs $\rho_{xx}{}^{1.6}$ plot, is a constant with respect to temperature, we collapse the curves into a single straight line by selecting the value of β in Eq. (A1). In the example illustrated by Fig. S4 the series of lines is collapsed to one line by choosing $\beta = 1.6$.

To further illustrate the importance of the domain coefficient β for our analysis, we plot (in the Supplemental Material [32]) the calculated and measured value of m as a function of

field B in Fig. S5. Figure S5(a) is again plotted with $\beta = 1.0$ for the same sample as in Fig. S4. Note that, although the theoretical and experimental curves converge at $B = 0$, as expected, they diverge very significantly as the field and temperature increases. However, with appropriately chosen β (in this case $\beta = 1.6$) the curves coalesce, as seen in Fig. S5(b). The agreement with just two adjustable parameters over such a wide range of temperatures and fields is truly remarkable, attesting to the effectiveness of the Weiss-Brillouin model as modified by Harrison. It is especially remarkable that the requirement of making the series of lines coalesce so as to give a single intercept has determined the value of $\beta = 1.6$, has automatically led to such excellent agreement of theory and experiment as illustrated in Fig. S5(b).

[1] T. Dietl, H. Ohno, and F. Matsukura, Hole-mediated ferromagnetism in tetrahedrally coordinated semiconductors, Phys. Rev. B **63**, 195205 (2001).

[2] T. Dietl and H. Ohno, Dilute ferromagnetic semiconductors: Physics and spintronic structures, Rev. Mod. Phys. **86**, 187 (2014).

[3] T. Dietl, A. Bonanni, and H. Ohno, Families of magnetic semiconductors — an overview, J. Semicond. **40**, 080301 (2019).

[4] T. Dietl, H. Ohno, F. Matsukura, J. Cibert, and D. Ferrand, Zener model description of ferromagnetism in zinc-blende magnetic semiconductors, Science **287**, 1019 (2000).

[5] A. H. MacDonald, P. Schiffer, and N. Samarth, Ferromagnetic semiconductors: Moving beyond (Ga,Mn)As, Nat. Mater. **4**, 195 (2005).

[6] S. Shen, X. Liu, Z. Ge, J. K. Furdyna, M. Dobrowolska, and J. Jaroszynski, Scaling of the anomalous Hall effect in low Mn concentration (Ga,Mn)As, J. Appl. Phys. **103**, 07D134 (2008).

[7] D. Chiba, A. Werpachowska, M. Endo, Y. Nishitani, F. Matsukura, T. Dietl, and H. Ohno, Anomalous Hall effect in field-effect structures of (Ga,Mn)As, Phys. Rev. Lett. **104**, 106601 (2010).

[8] P. Mitra, N. Kumar, and N. Samarth, Localization and the anomalous Hall effect in a dirty metallic ferromagnet, Phys. Rev. B **82**, 035205 (2010).

[9] T. Jungwirth, J. Sinova, J. Mašek, J. Kučera, and A. H. MacDonald, Theory of ferromagnetic (III,Mn)V semiconductors, Rev. Mod. Phys. **78**, 809 (2006).

[10] S. Onoda, N. Sugimoto, and N. Nagaosa, Quantum transport theory of anomalous electric, thermoelectric, and thermal Hall effects in ferromagnets, Phys. Rev. B **77**, 165103 (2008).

[11] M. Glunk, J. Daeubler, W. Schoch, R. Sauer, and W. Limmer, Scaling relation of the anomalous Hall effect in (Ga,Mn)As, Phys. Rev. B **80**, 125204 (2009).

[12] X. Liu, S. Shen, Z. Ge, W. L. Lim, M. Dobrowolska, J. K. Furdyna, and S. Lee, Scaling relations between anomalous Hall and longitudinal transport coefficients in metallic (Ga,Mn)As films, Phys. Rev. B **83**, 144421 (2011).

[13] A. Lemaître, A. Miard, L. Travers, O. Mauguin, L. Largeau, C. Gourdon, V. Jeudy, M. Tran, and J.-M. George, Strain control of the magnetic anisotropy in (Ga,Mn)(As,P) ferromagnetic semiconductor layers, Appl. Phys. Lett. **93**, 021123 (2008).

[14] A. W. Rushforth, M. Wang, N. R. S. Farley, R. P. Campion, K. W. Edmonds, C. R. Staddon, C. T. Foxon, and B. L. Gallagher, Molecular beam epitaxy grown (Ga,Mn)(As,P) with perpendicular to plane magnetic easy axis, J. Appl. Phys. **104**, 073908 (2008).

[15] M. Cubukcu, H. J. von Bardeleben, K. Khazen, J. L. Cantin, O. Mauguin, L. Largeau, and A. Lemaître, Adjustable anisotropy in ferromagnetic (Ga,Mn)(As,P) layered alloys, Phys. Rev. B **81**, 041202 (2010).

[16] X. Li, X. Liu, S. Dong, C. Gorsak, J. K. Furdyna, M. Dobrowolska, S.-K. Bac, S. Lee, and S. Rouvimov, Dependence of ferromagnetic properties on phosphorus concentration in $Ga_{1-x}Mn_xAs_{1-y}P_y$, J. Vac. Sci. Technol. B **36**, 02D104 (2018).

[17] S. Dong, L. Riney, X. Liu, L. Guo, R.-K. Zheng, X. Li, S.-K. Bac, J. Kossut, M. Dobrowolska, B. Assaf, and J K. Furdyna, Carrier localization in quaternary $Ga_{1-x}Mn_xAs_{1-y}P_y$ ferromagnetic semiconductor films, Phys. Rev. Mater. **5**, 014402 (2021).

[18] N. Nagaosa, J. Sinova, S. Onoda, A. H. MacDonald, and N. P. Ong, Anomalous Hall effect, Rev. Mod. Phys. **82**, 1539 (2010).

[19] R. Karplus and J. M. Luttinger, Hall effect in ferromagnetics, Phys. Rev. **95**, 1154 (1954).

[20] G. Sundaram and Q. Niu, Wave-packet dynamics in slowly perturbed crystals: Gradient corrections and Berry-phase effects, Phys. Rev. B **59**, 14915 (1999).

[21] Di Xiao, M.-C. Chang, and Q. Niu, Berry phase effects on electronic properties, Rev. Mod. Phys. **82**, 1959 (2010).

[22] S. Onoda, N. Sugimoto, and N. Nagaosa, Intrinsic Versus Extrinsic Anomalous Hall Effect in Ferromagnets, Phys. Rev. Lett. **97**, 126602 (2006).

[23] T. Jungwirth, Q. Niu, and A. H. MacDonald, Anomalous Hall Effect in Ferromagnetic Semiconductors, Phys. Rev. Lett. **88**, 207208 (2002).

[24] S. H. Chun, Y. S. Kim, H. K. Choi, I. T. Jeong, W. O. Lee, K. S. Suh, Y. S. Oh, K. H. Kim, Z. G. Khim, J. C. Woo, and Y. D. Park, Interplay between Carrier and Impurity Concentrations in Annealed $Ga_{1-x}Mn_xAs$: Intrinsic Anomalous Hall Effect, Phys. Rev. Lett. **98**, 026601 (2007).

[25] X.-J. Liu, X. Liu, and J. Sinova, Scaling of the anomalous Hall effect in the insulating regime, Phys. Rev. B **84**, 165304 (2011).

[26] C. Zeng, Y. Yao, Q. Niu, and H. H. Weitering, Linear Magnetization Dependence of the Intrinsic Anomalous Hall Effect, Phys. Rev. Lett. **96**, 037204 (2006).

[27] Qi Wang, Y. Xu, R. Lou, Z. Liu, M. Li, Y. Huang, D. Shen, H. Weng, S. Wang, and H. Lei, Large intrinsic anomalous Hall effect in half-metallic ferromagnet $Co_3Sn_2S_2$ with magnetic Weyl fermions, Nat. Commun. **9**, 3681 (2018).

[28] R. G. Harrison, Positive-feedback theory of hysteretic recoil loops in hard ferromagnetic materials, in IEEE Trans. Magn. **47**, 175 (2011).

[29] K. W. Edmonds, K. Y. Wang, R. P. Campion, A. C. Neumann, C. T. Foxon, B. L. Gallagher, and P. C. Main, Hall effect and hole densities in $Ga_{1-x}Mn_xAs$, Appl. Phys. Lett. **81**, 3010 (2002).

[30] Y. Pu, D. Chiba, F. Matsukura, H. Ohno, and J. Shi, Mott Relation for Anomalous Hall And Nernst Effects in $Ga_{1-x}Mn_xAs$ Ferromagnetic Semiconductors, Phys. Rev. Lett. **101**, 117208 (2008).

[31] D. Ruzmetov, J. Scherschligt, D. V. Baxter, T. Wojtowicz, X. Liu, Y. Sasaki, J. K. Furdyna, K. M. Yu, and W. Walukiewicz, High-temperature Hall effect in $Ga_{1-x}Mn_xAs$, Phys. Rev. B **69**, 155207 (2004).

[32] See Supplemental Material at http://link.aps.org/supplemental/10.1103/PhysRevB.103.214437 for the comparison between data of GaMnAsP and GaMnAs, and the magnetization fitting and analysis.

[33] M. Cubukcu, H. J. von Bardeleben, J. L. Cantin, I. Vickridge, and A. Lemaitre, Ferromagnetism in $Ga_{0.90}Mn_{0.10}As_{1-y}P_y$: From the metallic to the impurity band conduction regime, Thin Solid Films **519**, 8212 (2011).

[34] F. W. Van Keuls, X. L. Hu, H. W. Jiang, and A. J. Dahm, Screening of the Coulomb interaction in two-dimensional variable-range hopping, Phys. Rev. B **56**, 1161 (1997).

[35] W. Allen, E. G. Gwinn, T. C. Kreutz, and A. C. Gossard, Anomalous Hall effect in ferromagnetic semiconductors with hopping transport, Phys. Rev. B **70**, 125320 (2004).

[36] N. F. Mott, *Metal Insulator Transitions* (Taylor and Francis, London, 1974).

[37] A. L. Efros and B. I. Shklovskii, Coulomb gap and low temperature conductivity of disordered systems, J. Phys. C **8**, L49 (1975).

[38] Y. Imry, *Introduction to Mesoscopic Physics* (Oxford University Press, Oxford, 2002).

[39] L. Chen, S. Yan, P. F. Xu, J. Lu, W. Z. Wang, J. J. Deng, X. Qian, Y. Ji, and J. H. Zhao, Low-temperature magnetotransport behaviors of heavily Mn-doped (Ga,Mn)As films with high ferromagnetic transition temperature, Appl. Phys. Lett. **95**, 182505 (2009).

[40] S. Souma, L. Chen, R. Oszwaldowski, T. Sato, F. Matsukura, T. Dietl, H. Ohno, and T. Takahashi, Fermi level position, coulomb gap, and dresselhaus splitting in (Ga,Mn)As, Sci. Rep. **6**, 27266 (2016).

[41] Ye Yuan, C. Xu, R. Hübner, R. Jakiela, R. Böttger, M. Helm, M. Sawicki, T. Dietl, and S. Zhou, Interplay between localization and magnetism in (Ga,Mn)As and (In,Mn)As, Phys. Rev. Mater. **1**, 054401 (2017).

[42] M. Sawicki, D. Chiba, A. Korbecka, Yu. Nishitani, J. A. Majewski, F. Matsukura, T. Dietl, and H. Ohno, Experimental probing of the interplay between ferromagnetism and localization in (Ga, Mn)As, Nat. Phys. **6**, 22 (2010).

[43] M. Onoda and N. Nagaosa, Quantized Anomalous Hall Effect in Two-Dimensional Ferromagnets: Quantum Hall Effect in Metals, Phys. Rev. Lett. **90**, 206601 (2003).

[44] S. Raghu, X.-L. Qi, C. Honerkamp, and S.-C. Zhang, Topological Mott insulators, Phys. Rev. Lett. **100**, 156401 (2008).

[45] N. Samarth, Battle of the bands, Nat. Mater. **11**, 360 (2012).

[46] M. Dobrowolska, K. Tivakornsasithorn, X. Liu, J. K. Furdyna, M. Berciu, K. M. Yu, and W. Walukiewicz, Controlling the Curie temperature in (Ga,Mn)As through location of the Fermi level within the impurity band, Nat. Mater. **11**, 444 (2012).

[47] A. Richardella, P. Roushan, S. Mack, B. Zhou, D. A. Huse, D. D. Awschalom, and A. Yazdani, Visualizing critical correlations near the metal-insulator transition in $Ga_{1-x}Mn_xAs$, Science **327**, 665 (2010).

[48] M. Kobayashi, I. Muneta, Y. Takeda, Y. Harada, A. Fujimori, J. Krempaský, T. Schmitt, S. Ohya, M. Tanaka, M. Oshima, and V. N. Strocov, Unveiling the impurity band induced ferromagnetism in the magnetic semiconductor (Ga,Mn)As, Phys. Rev. B **89**, 205204 (2014).

[49] L. Montelius, S. Nilsson, and L. Samuelson, Characterization of the Mn acceptor level in GaAs, J. Appl. Phys. **64**, 1564 (1988).

[50] R. G. Harrison, A physical model of spin ferromagnetism, in IEEE Trans. Magn. **39**, 950 (2003).